J Mol Model (2007) 13:431–444
DOI 10.1007/s00894-006-0162-7

ORIGINAL PAPER

Effect of HPr phosphorylation on structure, dynamics, and interactions in the course of transcriptional control

Nadine Homeyer · Timm Essigke · Heike Meiselbach · G. Matthias Ullmann · Heinrich Sticht

Received: 19 July 2006 / Accepted: 4 October 2006 / Published online: 1 December 2006

Abstract The serine46-phosphorylated form of the bacterial protein HPr fulfils an essential function in carbon catabolite repression (CCR). Using molecular dynamics (MD) we studied the effect of Ser46 phosphorylation on the molecular properties of HPr and its capability to act as the co-repressor of carbon catabolite protein A (CcpA). The calculated pK_a values for a representative set of HPr(Ser46P) structures indicate that the phosphate group of HPr(Ser46P) exists predominately in the unprotonated form under neutral conditions. A hydrogen bond detected in HPr(Ser46P) between one phosphate-group oxygen and a side-chain hydrogen of Asn43—an amino acid conserved in all HPr proteins of Gram-positive bacteria that regulate their carbon consumption by CCR—might fulfil an important role in CcpA–HPr(Ser46P) complex formation. MD simulations show that the Ser46P–Asn43 hydrogen bond present in the unbound structure is replaced by intermolecular interactions upon complex formation. The degree to which amino acids in the CcpA–HPr(Ser46P) interface contribute to cofactor binding was analyzed by in silico alanine scanning. Lys307, Arg303, Asp296, Val300, and Tyr295 of CcpA were identified as important amino acids for the CcpA–HPr(Ser46P) interaction. Three of these residues are directly involved in sensing the correct phosphorylation state at His15(HPr) and Ser46(HPr). A substitution of interface residues Val319, Val314, Ser316, Leu321 and Gln320 by alanine showed that these amino acids, which contact helix α2 of HPr(Ser46P), play a less prominent role for complex formation.

Keywords HPr · Transcriptional control · Molecular dynamics · Alanine scan · pK calculation · Hydrogen bond

Electronic supplementary material Supplementary material is available in the online version of this article at http://dx.doi.org/10.1007/s00894-006-0162-7 and is accessible for authorized users.

N. Homeyer · H. Meiselbach · H. Sticht (✉)
Abteilung für Bioinformatik, Institut für Biochemie,
Friedrich-Alexander-Universität Erlangen-Nürnberg,
Fahrstraße 17,
91054 Erlangen, Germany
e-mail: h.sticht@biochem.uni-erlangen.de

T. Essigke · G. M. Ullmann
Structural Biology/Bioinformatics, Universität Bayreuth,
Universitätsstraße 30, BGI,
95447 Bayreuth, Germany

Introduction

Posttranslational, reversible phosphorylation of proteins plays a pivotal role in numerous cellular processes. Covalent binding of a phosphate group to a single amino acid can tremendously affect protein features and behavior. Changes induced by phosphorylation such as for example altered enzymatic activity, localization and binding affinity of proteins, are used to switch processes indispensable to life on or off. Among these processes are catabolic and metabolic pathways, signal transduction, growth, membrane transport, motor mechanisms and gene expression [1, 2].

In many Gram-positive bacteria, the phosphorylation state of histidine-containing phosphocarrier protein (HPr), a protein from the phosphoenolpyruvate: sugar phosphotransferase system (PTS), governs carbohydrate transport, metabolism and utilization. HPr can be phosphorylated at two different sites, His15 and Ser46. Phosphorylation at

His15 by phosphoenolpyruvate-dependent enzyme EI takes place in the PTS, responsible for the detection, uptake, and concomitant phosphorylation of carbohydrates [3, 4]. The Ser46-phosphorylated form of HPr is generated by an ATP-dependent HPr kinase/phosphatase (HPrK/P) [5] stimulated by high concentrations of glycolytic intermediates [6]. While HPr(His15P) serves mainly as a PTS phosphocarrier component and thus enables sugar consumption, HPr (Ser46P) mediates primarily carbon catabolite repression (CCR) via transcriptional control.

HPr(Ser46P) is an allosteric effector of the transcriptional regulator CcpA (carbon catabolite protein A). CcpA regulates a large number of genes that encode proteins involved in carbohydrate metabolism and utilization [7] by binding to catabolite-responsive elements (*cre*). Formation of the CcpA–HPr(Ser46P) complex, which consists of one CcpA dimer and two HPr(Ser46P) molecules, is necessary for a specific and high affinity CcpA–*cre* interaction [8]. Thus, binding of HPr(Ser46P) to CcpA triggers the regulation of *cre*-controlled genes. Since neither unphosphorylated HPr nor HPr(His15P) can bind to CcpA, CCR is exclusively governed by the Ser46 phosphorylation of HPr. Experimental data indicate that the expression of 8% of all *B. subtilis* genes is regulated by CcpA [7, 9]. Hence, CcpA–HPr(Ser46P)-governed transcription control has a genome-wide effect on the expression level of genes in low G+C Gram-positive bacteria.

CcpA consists of two domains, an N-terminal helix-turn-helix DNA-binding domain and a C-terminal effector-binding domain. HPr has the architecture of an open-faced four-stranded antiparallel β-sandwich that is flanked on one side by two long (α1, α3) and one short helix (α2) capped by Ser46. As evident from a crystal structure of the complex, the primary CcpA–HPr(Ser46P) interaction interface encompasses helices I and IX of CcpA as well as two helices and one turn of HPr(Ser46P) [10]. All residues of HPr(Ser46P) that contribute to the CcpA binding lie within two regions, contact region I (CRI) composed of HPr helix α1 with regulatory site residue His15 as well as the preceeding loop, and contact region II (CRII) comprising mainly helix α2 and Ser46P [11]. Although abundant information is available about the overall architecture of HPr and its general role in the course of carbon catabolite repression, little is known about the effects of Ser46 phosphorylation on HPr structure and dynamics. NMR-spectroscopic studies were hampered by the lack of hydrogens at the phosphate group [12], thus impeding direct detection of interactions formed by the phosphate via NOE distance constraints. Crystallographic structural information about the unbound form of Ser46-phosphorylated HPr is still limited to the structure of *E. faecalis* HPr [4]. The high B-factor of the phosphate group in this structure gives a first indication that this group might sample multiple conformations in the unbound form of HPr.

For a closer investigation of the effect of Ser46-phosphorylation on HPr structure and dynamics, we performed molecular-dynamics simulations of unphosphorylated and Ser46-phosphorylated HPr. Since the protonation state of the HPr Ser46 phosphate group in solution was unknown, simulations were performed for two different protonation states of the phosphate group. Subsequently, these simulations served as basis for pK_a value calculations. In addition to the studies of free HPr proteins, the conformational changes in HPr occurring during complex formation with CcpA were investigated by molecular-dynamics simulations of the appropriate complex.

Knowing that HPr binding to CcpA is greatly enhanced by the phosphorylation of HPr at Ser46 [13], it remains to be elucidated which features and amino acids of the transcription factor facilitate or enable complex formation. Although several CcpA mutants with an altered amino acid sequence in the cofactor binding region have been constructed and analyzed by experimental methods [14, 15], a global scan of the contact interface by single amino-acid substitutions has not yet been performed. Here we used the in silico alanine-scanning approach to study the influence of numerous binding-site residues in the CcpA–HPr(Ser46P) interaction.

Computational methods

Molecular-dynamics simulations

MD simulations were performed with the SANDER module of the AMBER 7.0 [16] suite of programs with the parm99 force field. [17, 18] The model proteins prepared for MD were neutralized by adding Na^+ ions. The neutral systems were solvated in a periodic TIP3P water box [19] with at least a 10 Å water shell between the solute and the border of the box. Parameters for singly protonated and unprotonated phosphoserine, missing in the AMBER parameter set, were assigned according to Homeyer et al. [20] All systems were minimized and equilibrated prior to MD production. First the positions of the solvent atoms were optimized, while the solute was restrained by a harmonic function with a force constant of 500 kcal mol^{-1} $Å^{-2}$. The relaxation of the solvent was carried out using 1,000 steps of steepest-descent minimization followed by 1,000 steps of the conjugate-gradient method. Subsequently, the whole system was minimized by again consecutively applying the two minimization algorithms. The temperature was then raised from 50 to 300 K during 80 ps equilibration MD. In the last stage of the preparation phase, a 50 ps MD run was conducted, in which the density of the systems was adjusted to 1 g cm^{-3}.

MD simulations were performed using a time step of 1 fs for the integration of the equations of motion. The particle-

mesh Ewald summation method was used for long-range electrostatic interactions. Short-range non-bonded interactions were truncated with a 10 Å cutoff. All bonds involving hydrogen atoms were constrained using the SHAKE procedure.

Production-phase MD simulations were carried out at 1 bar and 300 K under NPT conditions with a time constant of 2.5 ps for pressure relaxation. Snapshots of the systems were collected in time intervals of 1 ps along the trajectories. Results were analyzed and visualized using the programs X-PLOR[21], MOLMOL [22], SYBYL6.9 [23], and VMD [24].

Free HPr and HPr(Ser46P)

Eight Protein Data Bank (PDB) entries containing HPr structures from Gram-positive bacteria that possess CcpA and HPrK/P were selected for MD of free HPr. A total of ten HPr structures were extracted from these datasets and used for the analyses (cf. Table 1).

The G85R mutation present in the 1KKM and 1KKL structures was removed by deleting the Arg85 side-chain, and a M51V mutation present in the 1JEM structures was reversed by erasing the Val51 CG1 carbon and adding missing methionine atoms with the LEAP module of AMBER. Furthermore, the phosphate group of phosphohistidine15 was removed in the 1JEM structures prior to the actual model system preparations.

Two models representing either unphosphorylated HPr or HPr with doubly negative charged, unprotonated Ser46P (HPr-S2P) were generated from each structure listed in Table 1. Additionally, models of HPr with singly protonated Ser46P (HPr-S1P) were constructed from the four *B. subtilis* HPr structures. All model proteins were prepared for MD as described above. When the relaxation of the solvent had been completed, long minimizations of the whole systems were carried out in order to remove unfavorable conformations present in HPr structures taken from complexes, and/or caused by the addition of the phosphate group at position Ser46. Each protein system was subjected to 250 steps steepest-descent and 7,750 steps conjugate-gradient minimization. MD productions of the HPr and HPr-S2P models derived from *B. subtilis* HPr structures were carried out for a total of 9 ns. All other simulations of HPr, HPr-S1P and HPr-S2P were performed for a time period of 3 ns.

CcpA–HPr complexes

For an investigation of the structural features that influence the binding of HPr to CcpA as well as a characterization of the binding process and the interaction between the bound proteins, three CcpA–HPr complexes were constructed that represented $CcpA_{bound}$–HPr_{bound}, $CcpA_{unbound}$–$HPr_{unbound}$, and $CcpA_{bound}$–$HPr_{unbound}$ structures.

The $CcpA_{bound}$–HPr_{bound} complex used to analyze the dynamics and the interaction energetics in the bound state was generated by extracting a CcpA–HPr(Ser46P) structure, comprising one CcpA dimer and two HPr(Ser46P) molecules, from the complex crystal structure (PDB code: 1RZR).

To obtain a model $CcpA_{unbound}$–$HPr_{unbound}$ complex that can give information about the amino-acid arrangement in

Table 1 HPr structures used for MD simulations of free HPr and HPr(Ser46P) models

Model alias	PDB entry	Structure details	Species
KKL	1KKL [33]	HPr (chain J) from a crystal structure containing *B. subtilis* HPr in complex with *L. casei* HPrK/P	*Bacillus subtilis*
KKM	1KKM [33]	HPr with Ser46P (chain J) from a crystal complex structure consisting of *B. subtilis* HPr(Ser46P) and *L. casei* HPrK/P	*Bacillus subtilis*
JEM1	1JEM [41]	Model 1 from an ensemble of 25 HPr(His15P) NMR structures	*Bacillus subtilis*
JEM16	1JEM [41]	Model 16 from an ensemble of 25 HPr(His15P) NMR structures	*Bacillus subtilis*
FU0-A	1FU0 [4]	Crystal structure of HPr with Ser46P (chain A)	*Enterococcus faecalis*
FU0-B	1FU0 [4]	Crystal structure of HPr with Ser46P (chain B)	*Enterococcus faecalis*
PTF	1PTF [42]	HPr crystal structure	*Enterococcus faecalis*
QFR	1QFR [43]	Model 1 from an ensemble of 16 HPr structures determined by NMR spectroscopy	*Enterococcus faecalis*
KA5	1KA5 [44]	Model 1 from an ensemble of 16 HPr structures determined by NMR spectroscopy	*Staphylococcus aureus*
RZR	1RZR [10]	HPr with Ser46P (chain S) from a crystal structure of the ternary CcpA–HPr(Ser46P)-*cre* complex	*Bacillus megaterium*

the initial stage of the binding process, structures of unbound CcpA (PDB entry 1SXH) and unbound HPr were superimposed onto the appropriate subunits of the CcpA–HPr(Ser46P) complex from 1RZR using the backbone atoms of residues Thr60–Thr331 (CcpA) and Ala2–Glu88 (HPr). In this fit, two HPr structures recorded after 300 ps and 900 ps free MD served as models of the unbound HPr form.

The structural changes of HPr associated with CcpA-binding were analyzed by simulating the dynamics of a $CcpA_{bound}$–$HPr_{unbound}$ complex, composed of one CcpA dimer from 1RZR and two *B. megaterium* HPr(Ser46P) molecules that had previously been subjected to 1.5 ns free MD. This complex, henceforth termed CcpA–unboundHPr (Ser46P) complex, was generated by fitting the HPr molecules recorded during MD onto the backbone atoms of the HPr monomers of CcpA–HPr(Ser46P) from 1RZR and then deleting the bound HPr structures. The complex thus obtained was checked for clashes in the cofactor-binding interface with the program WHATCHECK [25]. Since all clashes could be removed by a short minimization, it was assumed that the complex constructed represented a stable structure that could be used for MD simulation.

Two of the three complexes constructed, CcpA–HPr (Ser46P) from 1RZR and CcpA–unboundHPr(Ser46P), were used for MD analyses. They were prepared for simulation as described above. Due to the size of the protein models, which consisted of 838 amino acids, the minimization of the systems was carried out for a total of 10,000 steps. MD structures were recorded during time periods of 400 ps and 1 ns for CcpA–HPr(Ser46P) and CcpA–unboundHPr(Ser46P), respectively.

p*K* calculations

Electrostatic energies were calculated from snapshots of the MD trajectories of HPr models JEM1 and JEM16 (Table 1) using programs based on the MEAD library. [26, 27] As mentioned above, the unprotonated (HPr-S2P) and the singly protonated (HPr-S1P) forms of Ser46P were simulated using MD to estimate if the simulated protonation form biases the results of the pK_a calculations. Since the structures obtained from the MD simulations mainly differed by the presence or absence of a Ser46P–Asn43 side-chain hydrogen bond, representative snapshots for the two conformations were analyzed separately.

AMBER charges [16] and Bondi radii [28] were used. Arg, Asp, Glu, Lys and phosphoserine where allowed to titrate using experimentally determined model pK_a values of 12.0, 4.0, 4.4, 10.4 and 6.0, respectively. For histidine, model pK_a values of 7.0 and 6.6 for the δ- and ε-tautomers were used. Calculations were performed for an ionic strength of 100 mM, a temperature of 300 K, and dielectric constants of 4 and 80 for the protein and the aqueous solution, respectively. Protonation probabilities were calculated from the electrostatic energies based on a Monte Carlo procedure as described previously [29]. p$K_{1/2}$ values of the sigmoidal protonation probability curves are given in Table 2. These can be compared to experimental pK_a values.

HPr alignment

Sequences of HPr proteins from 26 species that possess CcpA as well as HPrK/P and numerous species that lack either CcpA and/or HPrK/P were downloaded from the NCBI protein database. All derived sequences were aligned according to the ClustalW algorithm using the default settings of the input form at http://www.ch.embnet.org/software/ClustalW.html.

Alanine scanning of CcpA–HPr(Ser46P)

The trajectory recorded during the MD simulation starting from the CcpA–HPr(Ser46P) crystal-complex structure 1RZR ($CcpA_{bound}$–HPr_{bound} complex) was used for an alanine scan of the CcpA–cofactor interface. We calculated the relative change in free energy of binding ($\Delta\Delta G_{binding}$) for the alanine mutants of selected residues in CcpA–HPr (Ser46P) using a single-trajectory MM/PBSA approach [30, 31]. In the scan, the structures of the trajectory were mutated by truncating the side-chains of the residues one at a time. For the calculation, we followed the standard protocol described by Massova and Kollman [32], which assumes that the entropy of the mutant and the wild-type do not differ significantly, and therefore entropic contributions

Table 2 Calculated pK_a values of Ser46P in HPr-S2P (A) and HPr-S1P (B) structures recorded during MD simulations of JEM1 and JEM16

Structure	Ensemble 1: Ser46P hydrogen-bonded		Ensemble 2: Ser46P non-hydrogen-bonded	
	[a]MD time (ps)	pK_a	[a]MD time (ps)	pK_a
A				
JEM1	1,000	5.4	1,500	6.2
	4,000	5.7	5,500	6.2
JEM16	2,000	5.9	2,800	6.1
	3,500	6.0	5,000	5.9
B				
JEM1	2,300	6.0	500	6.8
	2,800	6.2	1,000	6.8
JEM16	1,600	6.6	500	6.6
	2,300	6.0	1,000	6.3

[a] time point in MD at which the structures were recorded

can be neglected in the calculation of $\Delta\Delta G_{binding}$. All CcpA residues within 6 Å of the HPr contact region II were consecutively replaced by alanine. Additionally, the CcpA amino acids that interact with phosphorylable His15(HPr) as well as CcpA residue Tyr295 were exchanged for alanine. Every snapshot recorded during the time interval 200–400 ps of the MD trajectory was analyzed.

Results and discussion

Effect of the phosphorylation state on HPr structure and dynamics

As it was the principal objective of this work to investigate the effect of HPr Ser46-phosphorylation, we first studied the phosphorylation-induced changes in the free protein using molecular-dynamics. HPr proteins from *B. subtilis* were chosen for the analysis because there are numerous different starting structures available (Table 1), thus allowing us also to address the effect of the starting structures on the results of the calculations. Simulations of HPr and HPr-S2P model proteins generated from four different *B. subtilis* HPr structures were conducted for 9 ns, in order to find out if and how the protein structure is affected by the presence of the Ser46 phosphate group.

Regardless of the original phosphorylation state, all HPr and HPr-S2P structures generated proved to be stable in MD simulations. The average root mean square deviation (RMSD) of the backbone atoms with respect to the MD starting structures ranged from 0.90 to 1.22 Å for the HPr and from 0.81 to 1.32 Å for the HPr(Ser46P) models. The HPr and HPr-S2P structures recorded along the trajectories were very similar. Figure 1 shows an overlay of the HPr and HPr-S2P snapshots collected after 9 ns MD of model KKM. The small differences in the geometries of the two structures were mainly restricted to the highly flexible loops as well as to the region of the short helix α2. A calculation of average backbone RMSDs between all final HPr and HPr-S2P snapshots yielded RMSD values ranging from 1.05 to 1.74 Å. Since the RMSDs between the unphosphorylated and phosphorylated structures lie only slightly above the RMSDs caused by the fluctuations within the protein systems, phosphorylation of Ser46 seems to have no great impact on the conformation of HPr. This result is in agreement with observations made in earlier structural analyses of *B. subtilis* HPr(Ser46P), which showed that HPr serine46 phosphorylation does not effect the overall geometry of the protein significantly [4, 12, 33].

In the next step, the arrangement of the amino acids in the neighborhood of Ser46P was analyzed. No general changes were detected in the average backbone dihedral angles ϕ and ψ of Ser46P and the adjacent residues (data not shown). A detailed analysis of the behavior of the amino-acid side-chains in the vicinity of Ser46P, however, revealed the presence of an interaction between Ser46P and the side-chain of Asn43. Measurements of distances and angles between atoms of the two side-chains showed that the asparagine hydrogen termed HD22 according to the AMBER nomenclature is frequently within hydrogen-bonding distance of one phosphate-group oxygen atom. The fact that different oxygens form the acceptor of the hydrogen bond indicates that the rotation of the phosphate group is not impeded by hydrogen bond formation (cf. Fig. 2). Using a distance smaller than 2.2 Å and an angle larger than 150° as hydrogen bond criteria, the number of structures that possess a hydrogen bond between Asn43 (HD22) and one phosphate group oxygen was calculated. Depending on the starting structure, the portion of this hydrogen-bonded conformation is in the range from 43 to 66% (Table 3), indicating that the choice of the starting structure does not have a major effect on the formation of this hydrogen bond. In all simulations, an alternative non-hydrogen-bonded conformation for Ser46P is observed, in which the phosphate group is oriented towards the solvent and does not form any intramolecular interactions.

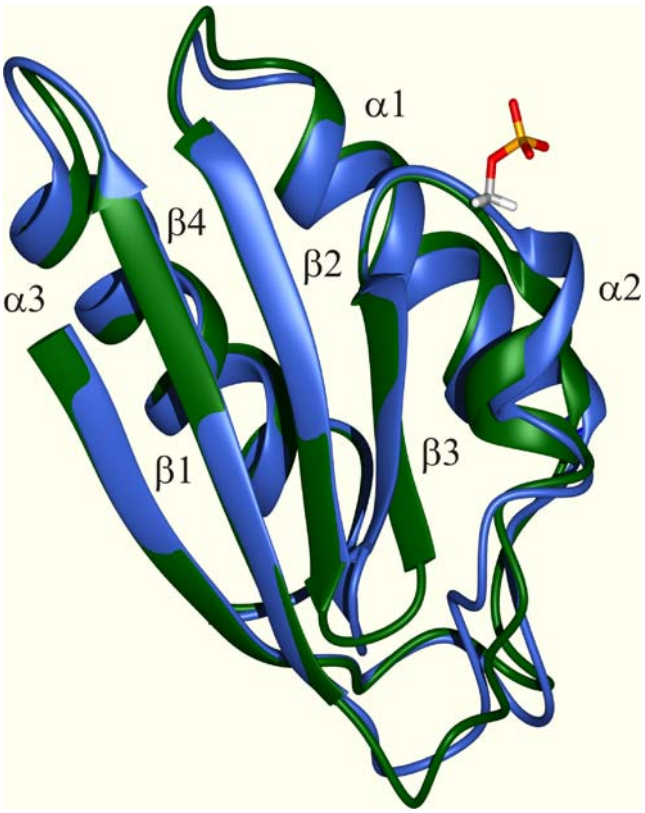

Fig. 1 Overlay of unphosphorylated HPr (*blue*) and HPr-S2P (*green*) after 9 ns MD of model KKM. Proteins are shown in cartoon representation, the secondary structure elements are indicated, and the atoms of the phosphorylated amino-acid are shown as *sticks*

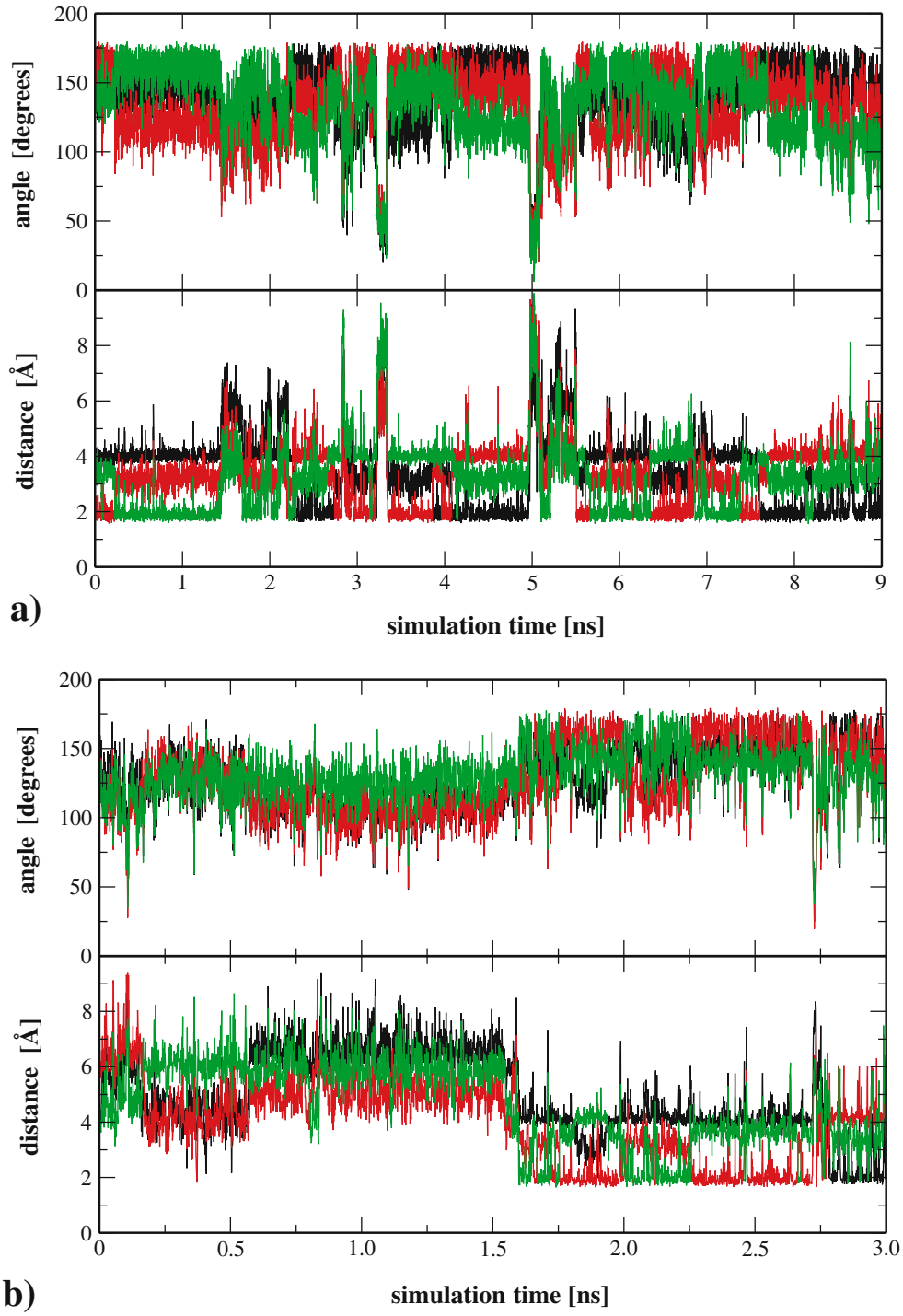

Fig. 2 Conformational sampling of HPr in different protonation states: Distances (*bottom*) and angles (*top*) between atoms involved in the Asn43(HD22)-Ser46P hydrogen bond during 9 ns MD of HPr-S2P (**a**) and 3 ns MD of HPr-S1P (**b**) for model JEM1. Asn43(ND2)-Asn43(HD22)-Ser46P(OXP) angles and Asn43(HD22)-Ser46P(OXP) distances for the phosphate group oxygens O1P, O2P, and O3P are colored in *black*, *red*, and *green*, respectively

Effect of the protonation state of Ser46P on HPr dynamics

One key prerequisite for the reliable interpretation of structures and conformational equilibria is the choice of the correct protonation state, which requires knowledge of the pK_a value of Ser46P in HPr. Until now, this pK_a value has not been determined experimentally, but studies of model peptides containing phosphoserine gave a pK_a of 5.96. [34] Since the protein environment in HPr might cause deviations from this value obtained for a short peptide fragment, it cannot a priori be ruled out that a portion of the protein exists in a singly protonated form at neutral pH. Since it is not easily possible to change the protonation state during MD simulations, four additional simulations were performed for the systems above, using a singly protonated form of Ser46P (S1P). Analysis of these

Table 3 Frequency of hydrogen bond presence during 9 ns as well as 3 ns MD simulations of HPr-S2P, and 3 ns simulations of HPr-S1P for four structures from *B. subtilis*; hydrogen bond criteria: Donor–acceptor distance smaller than 2.2 Å and O···H–N angle larger than 150°

Structure	Hydrogen bond presence (%)		
	HPr-S2P (9 ns MD)	HPr-S2P (3 ns MD)	HPr-S1P (3 ns MD)
JEM 1	65.52	63.20	29.93
JEM 16	48.29	69.20	24.27
KKL	43.22	32.43	29.40
KKM	52.86	51.27	3.67

simulations both gives information about the effect of the protonation state on the conformational equilibrium, and allows a calculation of the pK_a values for HPr(Ser46P).

One point that must also be considered in this context is the length of the simulations. The simulations described above for unsphosphorylated *B. subtilis* HPr and for the fully deprotonated, phosphorylated form (S2P) were run for 9 ns. Since these simulations are computationally very demanding, we first checked whether the conformational equilibrium between the non-hydrogen-bonded and hydrogen-bonded conformation of S2P can also be sampled adequately in shorter simulations. Table 3 compares the portion of hydrogen-bonded conformation present in the entire 9 ns trajectory of HPr-S2P with that found in the first 3 ns of the same simulation. The overall values are quite similar, and therefore we concluded that 3 ns simulations are sufficient for adequate sampling of the conformational equilibrium detected for HPr-S2P.

The 3 ns simulations performed for the singly protonated form (S1P) of *B. subtilis* HPr revealed that the protonation state of Ser46P does not affect the overall structure and dynamics of the protein (data not shown). As for the S2P simulations, a conformational equilibrium between a hydrogen-bonded and a non-hydrogen-bonded conformation was observed (cf. Fig. 2) but this equilibrium was shifted towards the non-hydrogen-bonded form (cf. Fig. 2; Table 3). The shift can be explained by the lower charges of the phosphate group oxygens in S1P compared to S2P, which decrease their ability to act as hydrogen-bond acceptors for the amide hydrogen of the Asn43 side-chain. A shift of the conformational equilibrium towards the non-hydrogen-bonded form of Ser46P was also observed in an earlier crystal structure of *E. faecalis* HPr(Ser46P), which was determined at high ionic strength (>1 M sodium/potassium phosphate) [4]. In this structure, the phosphate group of Ser46 is oriented towards the solvent, and according to the B-factor the phosphate is very flexible. This observation can most likely be attributed to the high ionic strength of the solute, which efficiently screens intramolecular electrostatic interactions, thus causing a similar effect as the decreased partial charges in the singly protonated form. A similar effect of high ionic strength in weakening electrostatic interactions was also reported for the binding of phosphotyrosine-containing peptides to the Syk SH2 domain [35].

Calculation of the pK_a of Ser46P in HPr

Since in silico pK_a calculations depend to a significant degree on the geometry of the input structures and the protonation state used in the simulations [36], analyses were performed for the non-hydrogen-bonded and the hydrogen-bonded conformations of Ser46P, and for both protonation states. In order to increase the statistical significance of the results, four snapshots originating from two different models (JEM1 and JEM16) were analyzed, resulting in a total of 16 structures (Table 2).

Generally, the hydrogen-bonded conformations exhibited lower pK_a values (ranging from 5.4 to 6.0 and from 6.0 to 6.6 for the S2P and S1P simulations, respectively). For the conformation without a hydrogen bond, pK_a values are slightly increased (5.9–6.2 and 6.3–6.8 for S2P and S1P, respectively), but are always below 7.0. The generally higher pK_a values for snapshots of the HPr-S1P trajectory compared to the HPr-S2P trajectory can be explained by the small bias that is introduced by the MD simulation. In the simulation of the protonated form, this form will be stabilized, which leads to an increased pK_a. Accordingly, in the pK_a calculations using the structures from the simulation of the deprotonated form, the pK_a is lowered [36]. However, the introduced bias is relatively small, allowing a reasonable estimate of the pK_a value of about 6. Assuming that the snapshots listed in Table 2 are representative for the ensemble, one can conclude that the S2P form is the predominant species at neutral pH with approximately 90%.

Conserved residues and interactions in HPr proteins from different bacterial species

The observation of an intramolecular side-chain hydrogen bond raises the question of the putative functional role of this interaction. If the interaction plays a general role, one would expect that the donor of the hydrogen bond is conserved among different bacterial species in which Ser46 becomes phosphorylated.

In order to analyze if the interaction observed can be formed in all HPr proteins of bacteria that are able to form serine phosphorylated HPr and use it for CCR regulation, HPr sequences of numerous organisms were compared by multiple sequence alignments. As can be seen in Fig. 3a, all HPr proteins studied from Gram-positive bacteria that

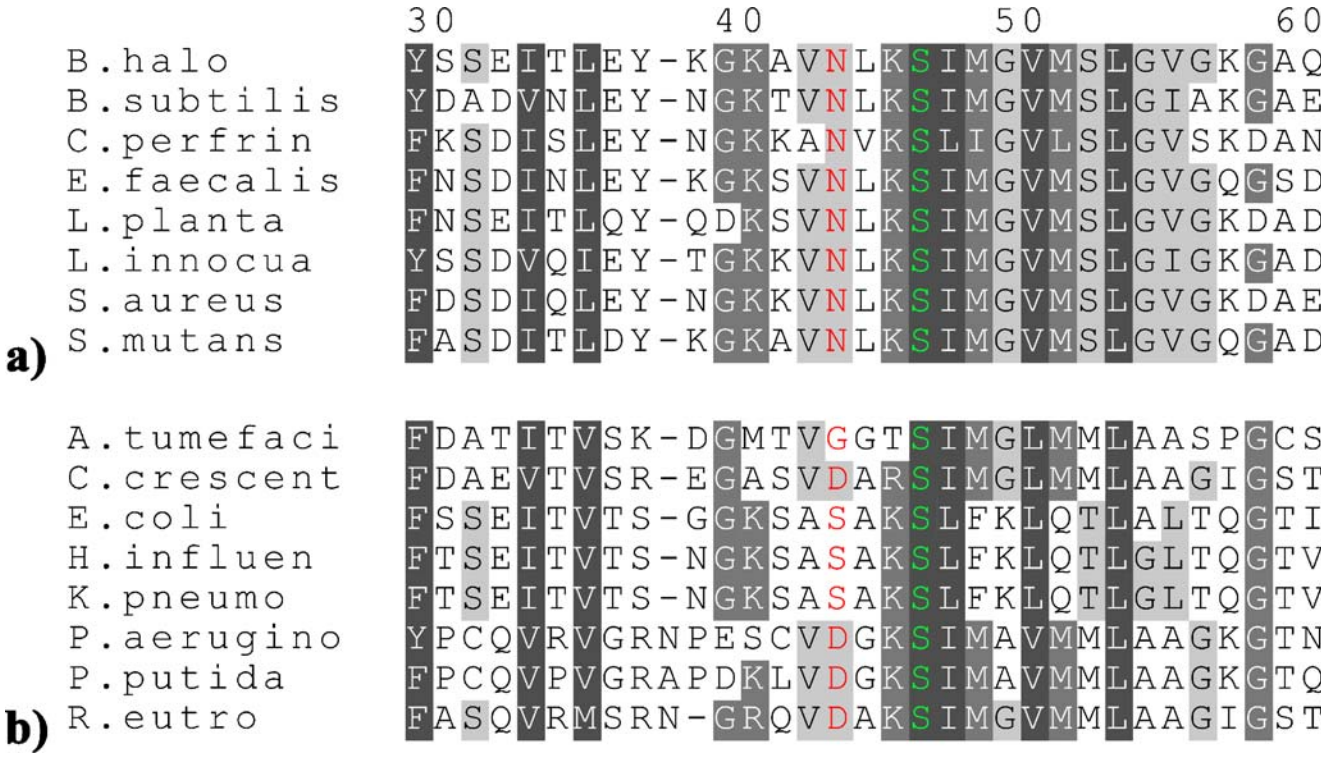

Fig. 3 Section of a multiple alignment of 16 HPr sequences, eight from Gram-positive (**a**), and eight from Gram-negative (**b**) bacterial species. The numbering scheme of *B. subtilis* HPr is given at the top. Phosphoserine residues and amino acids three positions ahead of the phosphorylation site are colored in *green* and *red*, respectively. Amino acids that are conserved in 100%, >80%, or >60% of the sequences are highlighted by *dark grey*, *medium grey*, and *light grey* boxes, respectively. Aliases stand for the following organisms/sequences: *A. tumefaci*: *Agrobacterium tumefaciens*/gi|17933955; *B.halo*: *Bacillus halodurans*/gi|15615636; *B.subtilis*: *Bacillus subtilis*/gi|48682; *C. crescent*: *Caulobacter crescentus*/gi|16124496; *C.perfrin*: *Clostridium perfringens*/gi|18310651; *E.coli*: *Escherichia coli*/gi|76365074; *E. faecalis*: *Enterococcus faecalis*/gi|287947; *H.influen*: *Haemophilus influenzae*/gi|1172745; *K.pneumo*: *Klebsiella pneumoniae*/gi|131536; *L.planta*: *Lactobacillus plantarum*/gi|28378035; *L.innocua*: *Listeria innocua*/gi|61230078; *P.aerugino*: *Pseudomonas aeruginosa*/gi|13633513; *P.putida*: *Pseudomonas putida*/gi|13633649; *R.eutro*: *Ralstonia eutropha*/gi|73540002; *S.aureus*: *Staphylococcus aureus*/gi|57651691; *S.mutans*: *Streptococcus mutans*/gi|24379147

possess HPrK/P as well as CcpA and are thus capable to control CCR via HPr(Ser46P) have an asparagine three positions ahead of the serine phosphorylation site. On the contrary, some of the HPr sequences from Gram-negative species that according to current knowledge lack either CcpA and/or HPrK/P have glycine (e.g. *Agrobacterium tumefaciens*), aspartic acid (e.g. *Pseudomonas aeruginosa*) or serine (e.g. *Escherichia coli*) at the appropriate sequence position (cf. Fig. 3b). It seems that the aspargine three residues ahead of the phosphorylation site has only been strictly conserved in HPr proteins of species that regulate their carbon consumption by HPr(Ser46P)-mediated CCR.

In order to find out if this conserved asparagine is capable of interacting with Ser46P not only in *B. subtilis* HPr but also in HPr proteins of other Gram-positive species that form HPr(Ser46P), simulations of HPr and HPr-S2P structures derived from *E. faecalis*, *B. megaterium* and *S. aureus* were performed. Again only minor differences were detected between the phosphorylated and the unphosphorylated protein systems. The backbone RMSDs between the HPr and the HPr-S2P structures recorded after 3 ns MD ranged from 1.23 to 1.85 Å. Since the structural variations during the simulations alone resulted in average backbone RMSDs of 0.95–1.40 Å for HPr-S2P, and 0.99–1.32 Å for HPr, it is obvious that the presence of the phosphorylated amino-acid Ser46P had no great influence on the protein architecture. Therefore, consistently with previous observations on *E. faecalis* HPr(Ser46P) [4] our results suggest that phosphorylation of serine46 generally has only a small effect on the geometry of HPr proteins from Gram-positive bacteria. In all model systems investigated, strong interactions were found between the side-chains of Asn43 and Ser46P. As in the simulations of *B. subtilis* HPr(Ser46P) a stable hydrogen bond was detected between one phosphate-group oxygen and the Asn43 hydrogen HD22 of the side-chain amide group. Table 4 gives an overview of the number of snapshots that fulfilled the hydrogen-bond criteria described previously. The Asn43–Ser46P hydrogen bond was present in at least 47.8% of all structures recorded during the 3 ns simulations. Thus, one can conclude that Asn43 is conserved in HPr proteins of those organisms in which Ser46 phosphorylated HPr can be used to trigger

Table 4 Frequency of hydrogen bond presence during 3 ns MD simulations of HPr-S2P model proteins derived from three Gram-positive species (see Table 1 for structure aliases); hydrogen bond criteria: Donor–acceptor distance smaller than 2.2 Å and O···H–N angle larger than 150°

Structure	Number of snapshots with Asn43(HD22)–Ser46P hydrogen bond				Hydrogen bond presence in percent
	Hydrogen bond acceptor			Σ	
	O1P	O2P	O3P		
FU0-A	932	181	582	1,695	56.5
FU0-B	438	275	784	1,497	49.9
PTF	109	1,258	607	1,974	65.8
QFR	706	680	410	1,796	59.9
KA5	1,131	287	16	1,434	47.8
RZR	1,098	957	35	2,090	69.7

CCR, and that the ability to form an Asn43–Ser46P hydrogen bond is also conserved among these organisms.

Interaction of HPr with CcpA

In order to gain a closer insight into the physiological role of the Asn43 conservation and the Asn43–Ser46P interaction, we performed a structural analysis of HPr in complex with the transcriptional regulator CcpA. An inspection of the *B. megaterium* CcpA–HPr(Ser46P) complex crystal structure (PDB entry 1RZR) [10] revealed that Asn43 is more than 7 Å apart from the CcpA surface, indicating that this residue is not directly involved in CcpA binding. However, an indirect role of Asn43 might result from its hydrogen-bonding capability. By forming a hydrogen bond with one phosphate oxygen, Asn43 could bring the phosphate group into a conformation favorable for CcpA-binding. To address this point, the non-hydrogen-bonded and hydrogen-bonded conformations of Ser46P were analyzed for their ability to interact with CcpA.

In the non-hydrogen-bonded conformation, Ser46P often adopts the same side-chain rotamer as in the crystal complex structure, suggesting that this conformation is favorable for binding, because binding does not require any rearrangement of the side-chain. In contrast, in most cases a change of the $\chi 1$ angle from −60° to 180° needs to take place upon binding in the hydrogen-bonded conformation. This consideration alone would suggest that the non-hydrogen-bonded form can interact more favorably with CcpA. However, the structural changes in CcpA upon binding of HPr(Ser46P) must also be considered, because binding of the non-hydrogen-bonded HPr form to unbound CcpA might cause steric clashes that cannot be deduced from the amino-acid arrangement in the complex structure. This is particularly important in the case of CcpA, which is known to undergo considerable structural changes upon HPr-binding as shown by comparison of the crystal structures of the unbound and bound CcpA form [10].

To gain information about the arrangement of the CcpA–HPr contact-region residues in the unbound proteins, structures of unbound CcpA and unbound HPr with and without an Asn43–Ser46P hydrogen bond were superimposed onto the appropriate subunits of the CcpA–HPr (Ser46P) complex crystal structure. This situation should closely resemble the initial recognition process of the free proteins in solution. The overlay revealed that the side-chain of Arg303(CcpA), which contacts Ser46P(HPr) directly in the CcpA–HPr complex [10], adopts a completely different conformation in the unbound protein (Fig. 4). This change of the Arg303 conformation between unbound and bound CcpA is mainly characterized by rotations of the side-chain angles $\chi 1$, $\chi 2$, and $\chi 3$. As shown in Fig. 4a, the non-hydrogen-bonded Ser46P is oriented towards the CcpA surface, and located very close to Arg303, while—due to the interaction of the phosphate group with Asn43(HPr)—it is positioned further away from Arg303(CcpA) in the overlay of the hydrogen-bonded structure (cf. Fig. 4b). These observations suggest that binding of an HPr conformer whose phosphate group is oriented towards the solvent might be unfavorable because Ser46P forms a lid on the Arg303 side-chain that hinders the Arg303 side-chain reorientation and thus the conformational changes required for CcpA repressor activity (Fig. 4a). In contrast, Ser46P of the hydrogen-bonded HPr conformation is located in a position that does not hinder Arg303 side-chain rearrangement, and allows concerted structural changes in HPr and CcpA upon complex formation (Fig. 4b).

A simulation of the formation of the 838-amino-acids complex starting from the free structures would be computationally too expensive, because the simulation would have to cover a long time period to allow the large structural rearrangements that occur in CcpA during allosteric activation [10]. Thus, computational studies are limited to an investigation of the structural changes that take place in HPr upon complex formation. In this context, it is of particular interest to clarify whether the intramolec-

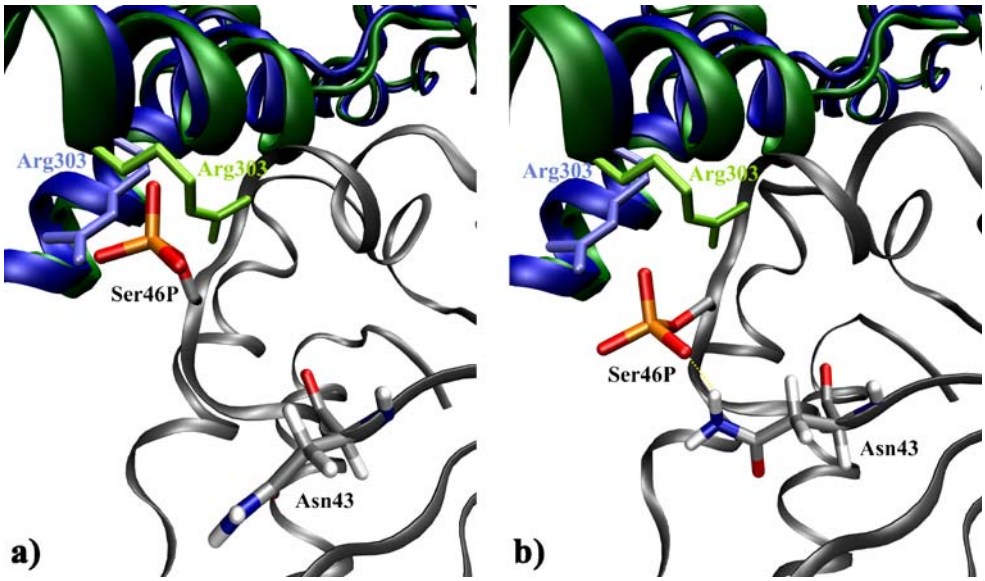

Fig. 4 Initial step of the HPr (*grey*)–CcpA (*green*) recognition. The different situations for the binding of the non-hydrogen-bonded HPr conformation (**a**) and the hydrogen-bonded HPr conformation (**b**) are shown. In order to visualize the structural changes in CcpA upon complex formation, the structure of free CcpA (*green*; PDB code 1SXH) was overlaid on the conformation of the complex crystal structure (*blue*; PDB code 1RZR). Note the rearrangement of the Arg303 side-chain is impeded by the HPr conformation in **a** but not by the conformation shown in **b**

ular Asn43–Ser46P interaction detected in HPr(Ser46P) can be replaced by the intermolecular interactions reported for the CcpA–HPr(Ser46P) complex. Therefore, we simulated the structural changes that occur in HPr upon complex formation by MD simulations starting from a hybrid complex constructed from the unbound HPr and bound CcpA conformation. This so-called "CcpA–unboundHPr (Ser46P)" complex was constructed by replacing the bound HPr(Ser46P) conformation in the complex crystal structure by an unbound *B. megaterium* HPr(Ser46P) structure with Asn43–Ser46P hydrogen bond, which was sampled during the MD simulations.

Figure 5 shows the unbound, hydrogen-bonded HPr (Ser46P) structure superimposed onto one HPr(Ser46P) monomer of the CcpA–HPr(Ser46P) complex. From the close-up view of the region around Ser46P it becomes obvious that a movement of the phosphate group towards Asn43 does not result in steric clashes with CcpA. The interaction between Asn43 and Ser46P positions the phosphate group further away from the surface of the CcpA dimer (cf. Figure 5). This is similar to the situation observed for the complex with the free CcpA conformation (cf. Fig. 4b).

In order to clarify if the intramolecular Asn43–Ser46P interaction detected in HPr(Ser46P) can be replaced by the intermolecular interactions reported for the CcpA–HPr (Ser46P) complex (1RZR) [10], we performed MD simulations of CcpA–HPr(Ser46P) and CcpA–unboundHPr (Ser46P). A detailed analysis of the CcpA–HPr(Ser46P) trajectory revealed that the intermolecular contacts between Ser46P and CcpA residues Arg303 and Lys307 present in 1RZR were mainly maintained during the whole simulation. Analogous contacts were formed in the CcpA–unboundHPr(Ser46P) equilibration MD, and proved to be stable in the course of the 1 ns simulation. Measurements of the distances between Ser46P and CcpA residues Arg303 and Lys307 revealed that the salt-bridges present in the crystal structure are reformed during the MD simulation that started from the CcpA–unboundHPr(Ser46P) complex structure (Fig. 6). An exact analysis of the relevant distances reveals the following changes (arrows denote the distance changes observed during 1 ns MD and the values in parenthesis give the corresponding distances in the complex

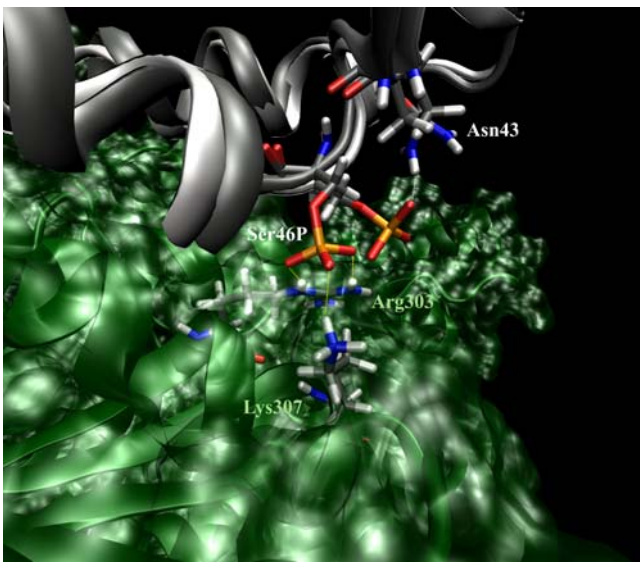

Fig. 5 Phosphate group interactions in the bound and unbound state of HPr(Ser46P). Overlay of the CcpA–HPr(Ser46P) complex crystal structure with HPr(Ser46P) after 1,500 ps free MD. Residues involved in hydrogen bonds with phosphate oxygens are shown in sticks representation. CcpA, bound HPr(Ser46P), and unbound HPr(Ser46P) are displayed as cartoons and colored in *green*, *dark grey* and *light grey*, respectively. Hydrogen bonds in the free HPr protein and in the complex are indicated by white and yellow dotted lines

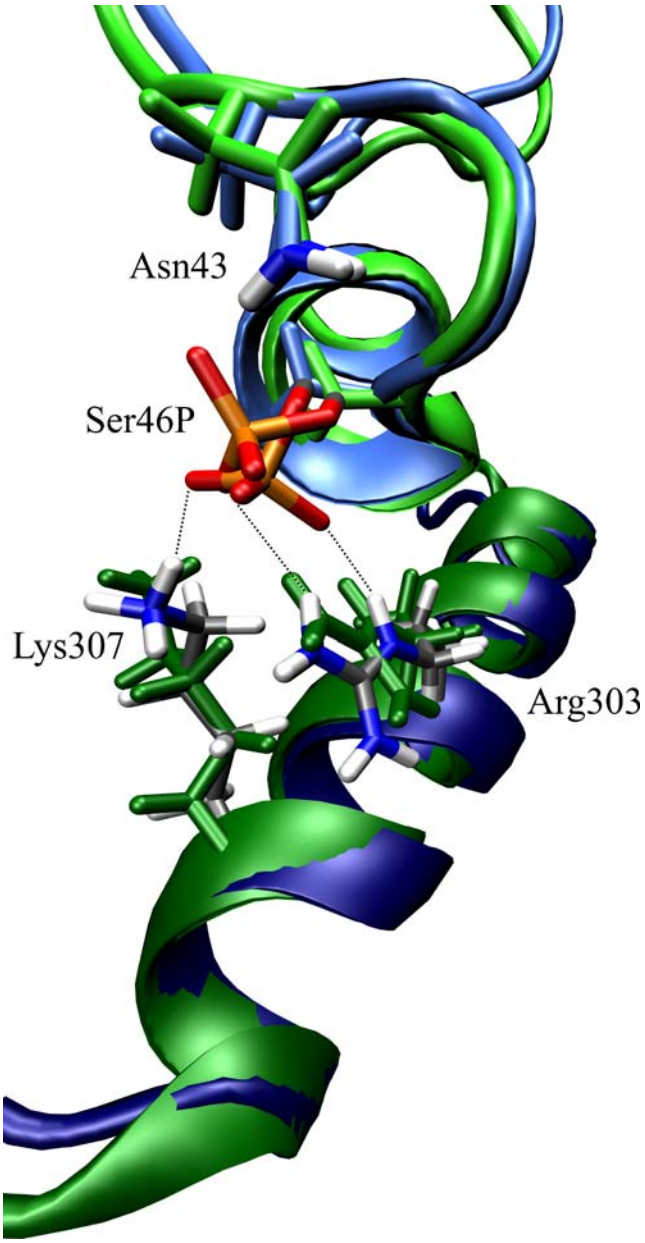

Fig. 6 Conformational changes in HPr upon complex formation. Overlay of modeled CcpA–unboundHPr(Ser46P) (*green*) and the structure after 1 ns MD (*blue*). Amino-acids 40–60 of HPr (*top*) and 290–315 of CcpA (*bottom*) are shown in detail. *Dotted lines* indicate the intermolecular electrostatic interactions formed after 1 ns MD, which are highly similar to those found in the complex crystal structure (see Fig. 5)

crystal structure): Arg303(NE)–Ser46P(OXP): 4.3 Å → 3.1 Å (3.2 Å), Arg303(NH2)–Ser46P(OXP): 3.3 Å → 2.7 Å (3.2 Å), and Lys307(NZ)–Ser46P(OXP): 4.0 Å → 2.7 Å (3.0 Å). Using a distance cutoff of 3.5 Å for the presence of a salt-bridge [37], these distances indicate that there is only one salt-bridge present at the start of the MD simulation, and that all three salt-bridges present in the complex crystal structure are re-established after 1 ns of simulation.

As can be seen in Fig. 6, which shows an overlay of the starting structure and that recorded after 1 ns MD, the phosphate group rotated about the Cβ–Oγ bond until it pointed towards CcpA residues Arg303 and Lys307. The intramolecular Asn43–Ser46P interaction became significantly weaker when the phosphate group moved in the direction of the CcpA dimer. From approximately 400 ps simulation onward, no phosphate oxygen came within hydrogen-bonding distance of an Asn43 side-chain hydrogen atom. These results indicate that the intramolecular interaction detected in unbound HPr(Ser46P) can be replaced by intermolecular interactions in the course of complex formation.

Identification of the CcpA-residues critical for HPr recognition

An additional objective of this work was to determine the main interactions that stabilize the CcpA–HPr(Ser46P) complex by in silico alanine scanning using an single-trajectory approach. Twelve amino acids of the CcpA–HPr interface were replaced by alanine according to the procedure described in the methods section. Their location is shown in Fig. 7. Four amino acids were identified as highly important for the interaction: Arg303, Lys307, Val300 and Tyr295. Substitution of these residues by alanine yielded negative $\Delta\Delta G_{\text{binding}}$ values below −2.0 kcal mol^{-1} (cf. Fig. 7). This means that an alanine in place of the respective residues is highly unfavorable. According to a previous definition [38], the magnitude of $\Delta\Delta G_{\text{binding}}$ is so high that the residues can be considered as 'hot spots' of the binding interface. The mutation of Asp296 to Ala also resulted in a significant decrease in free binding energy of more than 1 kcal mol^{-1}, which is at least twice as large as the effects for the remaining residues of the binding site (Table S1). Therefore, it can be assumed that Asp296 is also important for the CcpA–HPr interaction. Among the five amino acids identified as relevant for HPr binding were two residues (Arg303 and Lys307) that contact Ser46P of HPr directly [10]. As the favorable, polar interactions between these residues and Ser46P cannot be formed by alanine, it is reasonable that an alanine is highly unfavorable at both positions. Furthermore, it has been demonstrated experimentally that Arg303 is essential for HPr(Ser46P) binding [15].

Three amino acids of contact region I (CRI) were subjected to alanine scanning, Tyr295, Asp296 and Arg324. Tyr295, which was highly preferred to alanine, forms a hydrogen bond to the side-chain of HPr residue Thr20 in CcpA–HPr(Ser46P). A large decrease in free binding energy was expected for the Y295A mutant, not only because the favorable interaction is lost by the mutation, but also because Tyr295 had been reported to

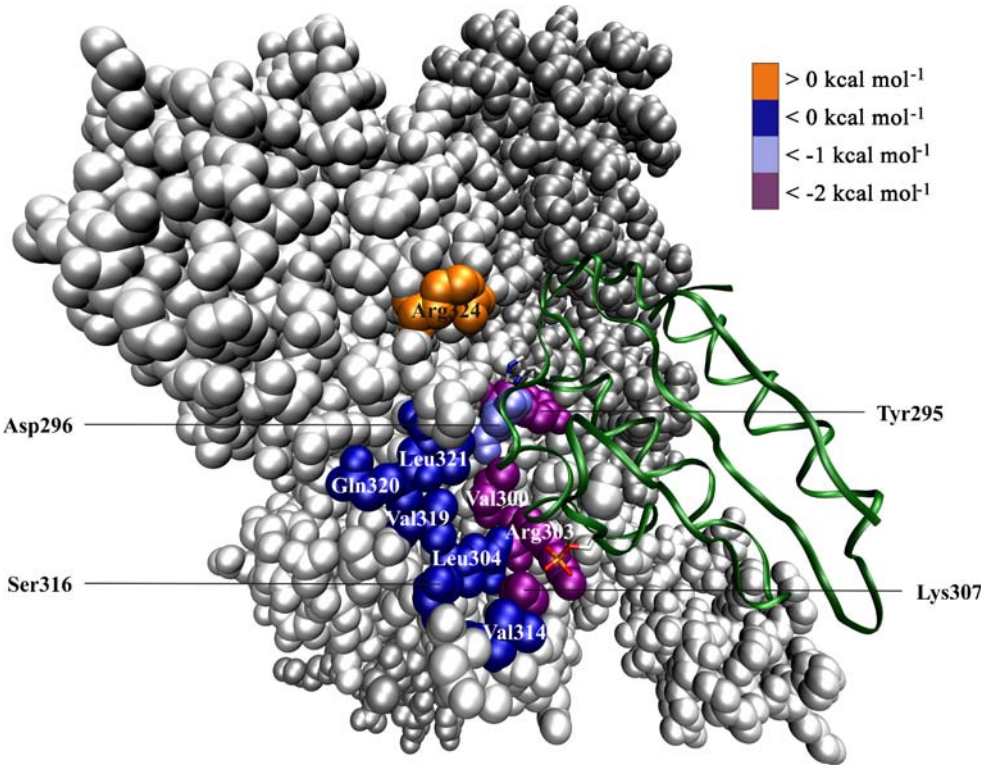

Fig. 7 Localisation of residues in the CcpA–HPr(Ser46P) interface that were substituted by alanine. The backbone of HPr is shown as *green ribbon* and the side-chains of Ser46P(HPr) and His15(HPr) are highlighted by CPK *colored sticks*. Both chains of the dimeric CcpA are shown in van der Waals presentation and are colored in *light grey* and *dark grey*, respectively. Amino-acids of CcpA that were subjected to alanine scanning are colored according to the calculated difference in free energy of binding between wild-type and mutant ($\Delta\Delta G_{binding}$)

be essential for CcpA–HPr(Ser46P) complex formation [15]. Arg324 and Asp296 are positioned close to HPr residue His15. While a substitution of Asp296 by alanine proved to be unfavorable, the Arg324 mutant yielded a large positive $\Delta\Delta G_{binding}$ value, suggesting that Ala is more favorable than the wild-type Arg for HPr binding. An explanation for this unexpected finding comes from the fact that this binding site is not only recognized by HPr, but also by its homologue Crh. The two proteins share a sequence identity of approximately 50% and the capability to become Ser46-phosphorylated, but differ at position 15 (histidine in HPr, glutamine in Crh). The negative $\Delta\Delta G_{binding}$ for Asp296 detected in our simulations is consistent with the crystal structures of the two complexes [10, 11], showing that Asp296 is important for the recognition of the side-chain N–H groups of His15 in HPr and Gln15 in Crh. In contrast, tight interactions between Arg324 and His15 of HPr, were neither observed in the crystal structure of CcpA–HPr(Ser46P) nor in our simulations, while the CcpA–Crh complex crystal structure [11] indicates a side-chain hydrogen bond between the guanidino-group of Arg324 and the amide group oxygen of Gln15. These findings suggest that Arg324 plays a unique role in Crh recognition, while it is dispensable for HPr recognition.

The last section of the interaction surface that was analyzed by in silico alanine scanning encompassed the CcpA region contacting helix α2 of HPr. Seven CcpA residues that lie within 6 Å of HPr were replaced consecutively by alanine. Only one of the seven mutants showed a significant decrease in free binding energy. The unpolar amino acid Val300, which is conserved in all CcpA family proteins [10], was highly preferred to alanine. A search in the Alanine Scanning Energetics database (ASEdb) [39] revealed that the observed $\Delta\Delta G_{binding}$ value of −2.76 kcal mol^{-1} for Val300Ala is among the highest found for Val to Ala mutations. As several mutagenesis studies have shown that the stability of a protein is destabilized by 1.5±0.5 kcal mol^{-1} per buried methylene group removed from an amino acid in the hydrophobic core [40], the calculated decrease in $\Delta G_{binding}$ is with ~1.4 kcal mol^{-1} per deleted methyl group in a magnitude typical for unpolar residues tightly buried in a hydrophobic environment. Thus, the decrease in free binding energy found for the Val300Ala mutation indicates that both methyl groups of Val300 are contacted by tightly packed hydrophobic residues of HPr in the interface. Indeed, HPr residues Ile47, Met48, and Met51, form tight contacts with Val300, which may be favored by the particular structural properties of the unbranched methionine side-chains.

It should be noted that the residue with the second largest $\Delta\Delta G_{binding}$ value among the seven mutated amino acids of the CcpA region contacting HPr helix α2 was Leu304. Although the effect of the Leu to Ala mutation seems to be relatively small compared to the Val300Ala mutation, it might nevertheless be significant, since Leu304 is also conserved in all proteins of the CcpA family [10].

We successfully identified five CcpA amino acids of the CcpA–HPr(Ser46P) interface that contribute significantly to

the affinity of complex formation. Three of them contact phosphorylation site residues known to be responsible for HPr binding regulation directly. These amino acids ensure that only HPr, unphosphorylated at His15 and phosphorylated at Ser46, is recognized by CcpA. Asp296 reads out the phosphorylation state of His15P, and Arg303 and Lys307 interact specifically with Ser46P. Thus, only few selective contacts enable a highly specific discrimination between different phosphorylation states of HPr.

Conclusion

We have investigated the effect of Ser46-phosphorylation of HPr on protein structure and dynamics as well as on its ability to interact with the transcriptional regulator CcpA. The MD simulations show that the phosphorylation itself has only minor effects on the overall HPr structure, and the calculated pK_a values indicate that the phosphate group of HPr(Ser46P) exists predominately in the unprotonated form at physiological pH. One of the orientations adopted by the phosphate group during the MD simulation is stabilized by a hydrogen bond to the side-chain amide proton of Asn43 and persists for approximately half of the simulation time. Asn43 is conserved in all Gram-positive bacteria that regulate their carbon consumption by CCR, and MD simulations of HPr proteins from different bacterial species that belong to this group confirm the presence of the Asn43–Ser46P hydrogen bond independently.

Modeling of the initial step of CcpA–HPr recognition suggests that the conformation stabilized by the hydrogen bond represents the binding-competent conformation because it does not hinder side-chain rearrangement in CcpA and allows concerted structural changes in both proteins upon complex formation. MD simulations show that the Ser46P–Asn43 hydrogen bond present in the unbound HPr structure is replaced by intermolecular interactions upon complex formation, which are highly similar to those reported previously for the CcpA–HPr(Ser46P) complex crystal structure.

A computational alanine scan of the CcpA–HPr interface identifies five residues (Lys307, Arg303, Asp296, Val300, and Tyr295) of CcpA as relevant for high-affinity binding. Three of them (Asp296, Arg303, Lys307) also play a crucial role for the discrimination between different phosphorylation states at His15(HPr) and Ser46(HPr), thus enhancing binding specificity.

Acknowledgements The authors thank the Regionales Rechenzentrum Erlangen for computational resources. This work was supported by a grant from the Deutsche Forschungsgemeinschaft (SFB473, C10) to H. Sticht. N. Homeyer acknowledges a fellowship from the BioMedTec International Graduate School of Science (BIGSS), supported by the state of Bavaria.

References

1. Tholey A, Lindemann A, Kinzel V, Reed J (1999) Biophys J 76:76–87
2. Johnson LN, Lewis RJ (2001) Chem Rev 101:2209–2242
3. Postma PW, Lengeler JW, Jacobson GR (1993) Microbiol Rev 57:543–594
4. Audette GF, Engelmann R, Hengstenberg W, Deutscher J, Hayakawa K, Quail JW, Delbaere LT (2000) J Mol Biol 303:545–553
5. Deutscher J, Saier MH Jr (1983) Proc Natl Acad Sci USA 80:6790–6794
6. Titgemeyer F, Hillen W (2002) Antonie Van Leeuwenhoek 82:59–71
7. Moreno MS, Schneider BL, Maile RR, Weyler W, Saier MH Jr (2001) Mol Microbiol 39:1366–1381
8. Jones BE, Dossonnet V, Kuster E, Hillen W, Deutscher J, Klevit RE (1997) J Biol Chem 272:26530–26535
9. Lorca GL, Chung YJ, Barabote RD, Weyler W, Schilling CH, Saier MH Jr (2005) J Bacteriol 187:7826–7839
10. Schumacher MA, Allen GS, Diel M, Seidel G, Hillen W, Brennan RG (2004) Cell 118:731–741
11. Schumacher MA, Seidel G, Hillen W, Brennan RG (2006) J Biol Chem 281:6793–6800
12. Pullen K, Rajagopal P, Branchini BR, Huffine ME, Reizer J, Saier MH Jr, Scholtz JM, Klevit RE (1995) Protein Sci 4:2478–2486
13. Seidel G, Diel M, Fuchsbauer N, Hillen W (2005) FEBS J 272:2566–2577
14. Kraus A, Hillen W (1997) FEMS Microbiol Lett 153:221–226
15. Kraus A, Kuster E, Wagner A, Hoffmann K, Hillen W (1998) Mol Microbiol 30:955–963
16. Case DA, Pearlman DA, Caldwell JW, III TEC, Wang J, Ross WS, Simmerling CL, Darden TA, Merz KM, Stanton RV, Cheng AL, Vincent JJ, Crowley M, Tsui V, Gohlke H, Radmer RJ, Duan Y, Pitera J, Massova I, Seibel GL, Singh UC, Weiner PK, Kollman PA (2002) Amber 7 University of California, San Francisco, USA
17. Cornell WD, Cieplak P, Bayly CI, Gould IR, Merz KM Jr, Ferguson DM, Spellmeyer DC, Fox T, Caldwell JW, Kollman PA (1995) J Am Chem Soc 117:5179–5197
18. Cheatham TE, 3rd, Cieplak P, Kollman PA (1999) J Biomol Struct Dyn 16:845–862
19. Jorgensen WL, Chandrasekhar J, Madura JD, Impey RW, Klein ML (1983) J Chem Phys 79:926–935
20. Homeyer N, Horn AH, Lanig H, Sticht H (2006) J Mol Model (Online) 12:281–289
21. Brünger AT (1992) Yale University Press, New Haven, CT
22. Koradi R, Billeter M, Wuthrich K (1996) J Mol Graph 14:51–55, 29–32
23. Tripos (1991–2002) Sybyl 6.9, Release 7.0A. St. Louis, Missouri, USA
24. Humphrey W, Dalke A, Schulten K (1996) J Mol Graph 14:33–38, 27–38
25. Hooft RW, Vriend G, Sander C, Abola EE (1996) Nature 381:272
26. Bashford D, Gerwert K (1992) J Mol Biol 224:473–486
27. Bashford D (1997) In: Ishikawa Y, Oldehoeft RR, Reynders JVW, Tholburn M (eds) Scientific Computing in Object-oriented Parallel Environments, ISCOPE97, Marina del Rey, CA, USA, December 8–11, 1997, Proceedings, vol 1343. Springer, Berlin, p 233–240
28. Bondi A (1964) J Phys Chem 68:441–451
29. Ullmann GM, Knapp EW (1999) Eur Biophys J 28:533–551
30. Srinivasan J, Miller J, Kollman PA, Case DA (1998) J Biomol Struct Dyn 16:671–682
31. Lepsik M, Kriz Z, Havlas Z (2004) Proteins 57:279–293
32. Massova I, Kollman PA (1999) J Am Chem Soc 121:8133–8143

33. Fieulaine S, Morera S, Poncet S, Mijakovic I, Galinier A, Janin J, Deutscher J, Nessler S (2002) Proc Natl Acad Sci USA 99:13437–13441
34. Bienkiewicz EA, Lumb KJ (1999) J Biomol NMR 15:203–206
35. Grucza RA, Bradshaw JM, Mitaxov V, Waksman G (2000) Biochemistry 39:10072–10081
36. Wlodek ST, Antosiewicz J, McCammon JA (1997) Protein Sci 6:373–382
37. Meiselbach H, Sticht H, Enz R (2006) Chem Biol 13:49–59
38. Bogan AA, Thorn KS (1998) J Mol Biol 280:1–9
39. Thorn KS, Bogan AA (2001) Bioinformatics 17:284–285
40. Wallis R, Leung KY, Osborne MJ, James R, Moore GR, Kleanthous C (1998) Biochemistry 37:476–485
41. Jones BE, Rajagopal P, Klevit RE (1997) Protein Sci 6:2107–2119
42. Jia Z, Vandonselaar M, Hengstenberg W, Quail JW, Delbaere LT (1994) J Mol Biol 236:1341–1355
43. Maurer T, Doker R, Gorler A, Hengstenberg W, Kalbitzer HR (2001) Eur J Biochem 268:635–644
44. Maurer T, Meier S, Kachel N, Munte CE, Hasenbein S, Koch B, Hengstenberg W, Kalbitzer HR (2004) J Bacteriol 186:5906–5918